Supplemental material: Topological classification for intersection singularities of exceptional surfaces in pseudo-Hermitian systems

Hongwei Jia[#], Ruo-Yang Zhang[#], Jing Hu, Yixin Xiao, Yifei Zhu[*], C. T. Chan[†]

1. Pseudo-Hermiticity and metric operator

The pseudo-Hermiticity can be regarded as a symmetry in non-Hermitian physics [1], and a formal definition of pseudo-Hermiticity is always accompanied with a metric operator η

$$\eta H \eta^{-1} = H^{\dagger} \tag{S1}$$

Hence, a pseudo-Hermitian system is also called a η-pseudo-Hermitian system, and the metric operator η is a Hermitian matrix. Recently, the parity-time inversion symmetry (*PT*) is included in pseudo-Hermiticity symmetry [2,3]. The considered system thus includes two inequivalent pseudo-Hermitian symmetries. In quantum mechanics, the Hamiltonians of two systems can be considered to be equivalent if they can transform to each other via unitary transformations ($U^{-1} = U^{\dagger}$)

$$H\varphi = E\varphi \rightarrow UHU^{\dagger}U\varphi = EU\varphi \rightarrow H'\varphi' = E\varphi' \tag{S2}$$

We apply the transformation to Eq. S1

$$\begin{aligned} & U\eta H\eta^{-1}U^{\dagger} = UH^{\dagger}U^{\dagger} \\ & \rightarrow U\eta U^{\dagger}UHU^{\dagger}U\eta^{-1}U^{\dagger} = UH^{\dagger}U^{\dagger} \\ & \rightarrow \eta' H' \eta'^{-1} = H'^{\dagger} \end{aligned} \tag{S3}$$

where $\eta' = U\eta U^{\dagger}$ is the transformed metric operator. For the considered system in Eq. (S2), one can apply an SU(2) transformation to the Hamiltonian, e.g.

$$\begin{aligned} & H' = e^{i\frac{\theta}{2}\sigma_1} H e^{-i\frac{\theta}{2}\sigma_1} \\ & = (f_2(\mathbf{k})i\sigma_2 + f_3(\mathbf{k})\sigma_3)\cos\theta + (-f_2(\mathbf{k})i\sigma_3 + f_3(\mathbf{k})\sigma_2)\sin\theta \end{aligned} \tag{S4}$$

It is found that the Hamiltonian can be transformed to a *PT*-symmetric system with equal gain and loss for $\theta = \pi/2$,

$$H' = -f_2(\mathbf{k})i\sigma_3 + f_3(\mathbf{k})\sigma_2 \tag{S5}$$

and the metric operator is simultaneously transformed to

$$\eta' = \begin{bmatrix} 0 & i \\ -i & 0 \end{bmatrix} \tag{S6}$$

Hence, the classification in this work can be extended to other *PT*-symmetric pseudo-Hermitian systems (e.g. realized by equal gain and loss, Eq. S5) with equivalent metric operators [4].

2. Quotient space and stratified space

In topology, the quotient space of a topological space under given equivalence relations is a new topological space constructed by endowing the quotient set of the original topological space with the quotient topology [5]. Let (X, τ_X) be a topological space, and let ~ be equivalent relation on X. The quotient set $Y=X/\sim$ is the set of equivalence classes of elements of X. The equivalence class of $x \in X$ is denoted by $[x]$. The quotient map associated with ~ refers to the surjective map

$$\begin{aligned} q: X &\to X/\sim \\ x &\to [x] \end{aligned} \tag{S7}$$

Intuitively speaking, all pointsin each equivalence class are identified or glued together. A well-known example of quotient space is the Brillouin zone. In the momentum space of periodic systems, a point $\mathbf{k}$ is identified with points $\mathbf{k}+m_a\mathbf{G}_a$ because a $\mathbf{k}$-space Hamiltonian at these points have the same eigenvalues and eigenstates. Here $\mathbf{G}_a$ are reciprocal lattice vectors and m_a are integers. That is why we mostly considers the band dispersions in the first Brillouin zone. It is also notable that the points on one side of the Brillouin zone boundaries can be translated to the points on the other boundary under translational operations of $\mathbf{G}_a$. Such points are identified and can be glued together. As simple examples, the first Brillouin zone is a quotient map of the momentum space under equivalence relation of translations by $\mathbf{G}_a$, and points in the first Brillouin zone are the representatives of all the equivalence classes. For 1D periodic systems, identifying points on the first Brillouin zone boundary constructs a quotient space, which is a 1D circle S^1 (see Fig. S1a1-a2). Similarly, opposite edges (p_1 and p_2, and p_3 and p_4) of the Brillouin zone of 2D periodic systems can be identified (see Fig. S1b1). By gluing p_1 to p_2, the Brillouin zone becomes a cylinder (see Fig. S1b2). We further glue p_3 to p_4, and the cylinder becomes a torus T (see Fig. S1b3). p_1 (or p_2) and p_3 (or p_4) are called the skeleton of the torus, and is a bouquet of two circles with a common basepoint $S^1 \vee S^1$. The surface of the torus is called the two-cell. Assembling the skeleton and the two-cell, the torus can be described by the product $T = S^1 \times S^1$. The topology of the torus is thus described by its fundamental group $\pi_1(T) = \mathbf{Z} \times \mathbf{Z}$. This is a free Abelian group on two generators.

The momentum space of the considered system is a stratified space [6,7]. In topology, a stratified space is a triple (V,S,ζ), where V is a topological space (often we require it to be locally compact, Hausdorff, and second countable), S is a decomposition of V into strata $V = \bigcup_{X \in S} X$, and ζ is the set of control data $\{(T_X),(\pi_X),(\rho_X) | X \in S\}$, where T_X is an open neighborhood of the stratum X, π_X: $T_X \to X$ is a continuous retraction, and ρ_X: $T_X \to [0,+\infty)$ is a continuous function. These data need to satisfy the following conditions:

1. Each stratum X is a locally closed subset and the decomposition S is locally finite.

2. The decomposition S satisfies the axiom of the frontier: if X, $Y \in S$ and $Y \cap \bar{X} \neq \varnothing$, then $Y \subset \bar{X}$. The condition implies that there is a partial order among strata: $Y<X$ if and only if $Y \subset \bar{X}$ and $Y \neq X$.

3. Each T_X is a smooth manifold.

4. $X=\{v \in T_X | \rho_X(v)=0\}$. So ρ_X can be viewed as the distance function from the stratum X.

5. For each pair of strata $Y<X$, the restriction (π_X, ρ_X): $T_Y \bigcap X \to Y \times (0,+\infty)$ is a submersion.

6. For each pair of strata $Y<X$, there holds $\pi_Y \circ \pi_X = \pi_Y$ and $\rho_Y \circ \pi_X = \rho_Y$.

Consider the parameter space f_2-f_3 of our Hamiltonian, the topological space V is simply the plane (Fig. S2). Thus S is the decomposition of V into three strata (X, Y, Z), which are the 2D space R^2 (X), the

singular hypersurfaces ELs at $f_2 = \pm f_3$ (Y=Sing(X)), and the hypersurface singularity NIP (Z=Sing(Sing(X))) at the center, as shown in Fig. S2. For each stratum (e.g. X), the smooth manifold T_X considers the nearby neighborhood. Therefore, T_1-T_3 in Fig. S2 correspond to the three strata X, Y and Z, respectively.

Our classification is based on eigenstates. The Hamiltonian in spaces without gap closing can be expressed with the sum

$$H = \sum_{i=1,2} E_i \left|\varphi_i^L\right\rangle\left\langle\varphi_i^R\right| \tag{S8}$$

where $\varphi_i^{L(R)}$ denote the left and right eigenstates of the Hamiltonian. The pseudo-Hermiticity and PT symmetries of the system enforces the left and right eigenstates (both in exact and broken phases) to be connected by the following relation

$$\varphi_i^L = \eta(\varphi_i^R)^* \tag{S9}$$

The quotient space is constructed by identifying points with the same eigenstates. Note that the eigenstates are ordered by the corresponding eigenvalues, and the criterion for ordering eigenstates has been introduced in the maintext. Hence, gluing point A' and point A, and B to B' is understandable, because the two eigenstates at these points coalesce, and ordering eigenstates is meaningless at these points.

$$\begin{aligned} \varphi_1 = \varphi_2 = \begin{bmatrix} -1 \\ 1 \end{bmatrix} \quad & for \;\; f_2 = f_3 \\ \varphi_1 = \varphi_2 = \begin{bmatrix} 1 \\ 1 \end{bmatrix} \quad & for \;\; f_2 = -f_3 \end{aligned} \tag{S10}$$

However, in spaces without gap closing, by adding a minus sign to the Hamiltonian in Eq. S8, both eigenenergies take negative signs, and the eigenstates remain the same. This process can be realized by taking the negatives of f_2 and f_3, which are just the antipodal points lying in opposite regions with respect to the NIP. Even though the two points have the same eigenstates, the order of the two states exchanges for antipodal points because eigenvalues are added by minus signs. Therefore, the two points cannot be identified, which is distinct from the points on ELs. The constructed space Eq. (3) in the main text is a stratified quotient space, and the corresponding topology Eq. (4) is thus a quotient space topology. Since the nontrivial loops in parameter (or quotient) space all traverses the singular hypersurfaces (i.e. EL or ES), our approach is affiliated to the intersection homotopy theory [6].

3. Frame deformation of eigenstates

The metric operator for pseudo-Hermiticity plays a similar role as the space-time metric in general relativity [8,9], and the eigenstates are like local coordinate frames (or tetrad). The local metric g can be defined with the indefinite inner product $g_{mn} = \left\langle\varphi_m \,|\, \eta\varphi_n\right\rangle$ [10]. The symmetries provide an orthogonality relation to the right eigenstates

$$\varphi_m^T \eta \varphi_n \begin{cases} = 0 & m \neq n \\ \neq 0 & m = n \end{cases} \tag{S11}$$

Since the Hamiltonian is gauged to be real, the eigenstates are real by removing arbitrary phases in exact phases ($|f_3|>|f_2|$), and thus the eigenstates in *PT*-exact phases have another orthogonal relation

$$\left\langle \varphi_m \,|\, \eta\varphi_n \right\rangle \begin{cases} = 0 & m \neq n \\ \neq 0 & m = n \end{cases} \tag{S12}$$

meaning that g is a diagonal metrix. However, the two diagonal elements of g have opposite signs, i.e. one vector is space-like and the other is time-like, which imposes the Riemannian geometry [i.e. SO(1,1) transformation] of the evolution of eigenstates as parameters vary. It is notable that in a specific region, g is invariant. In our previous work discussing the topology of swallowtail catastrophes in non-Hermitian systems [10], we established the relationship between the local metric g and the geometric phase. Here we will not repeat the derivation details, and we simply use the relationship between the metric g and the affine connection of the geometric phase

$$A^{*\,l}_{k_i\ m} g_{ln} + g_{ml} A_{k_i}^{\ \ l}{}_{n} = 0 \tag{S13}$$

to predict the emergence of ELs and NIPs. The affine connection is defined by the eigenstates

$$A_{k_i}^{\ \ n}{}_{m} = -\left\langle \varphi_n \left| \eta \frac{\partial}{\partial k_i} \right| \varphi_m \right\rangle \tag{S14}$$

More details can be found in [10].

In *PT*-exact phases, the local metrics in Region I and Region III are in the following forms

$$g_{\mathrm{I}} = \begin{bmatrix} 1 & 0 \\ 0 & -1 \end{bmatrix}, \quad g_{\mathrm{III}} = \begin{bmatrix} -1 & 0 \\ 0 & 1 \end{bmatrix} \tag{S15}$$

Here the sequence of eigenvalues is defined by sorting the corresponding eigenvalues from small to large. The geometric phase is an integration of the affine connection

$$U^{-1} = \mathrm{P}\exp\left(\int_{\mathbf{k}(0)}^{\mathbf{k}(\xi)} d\mathbf{k} A_{\mathbf{k}}\right) \tag{S16}$$

where P is the path ordering operator because the affine connection is a matrix. It is not difficult to find out that the two eigenstates experience Lorentz boost and the geometric phase is simply

$$U^{-1} = \exp \gamma T \tag{S17}$$

where T is the Lie algebraic generator of SO(1,1) group

$$T = \begin{bmatrix} 0 & 1 \\ 1 & 0 \end{bmatrix} \tag{S18}$$

and can be derived from Eq. (S13-14). Next, we define the path parameter θ (see Fig. S3a), with $f_3 = \cos\theta$ and $f_2 = \sin\theta$. The evolution of eigenvalues and eigenstates along the path α ($-\pi/4 \le \theta \le \pi/4$) is shown in Fig. S3b1 and b2, respectively. Note that the eigenstates have been rescaled. As can be indicated in Fig. S3b2, the two eigenstates are rotating in opposite directions, and resultantly, they evolve from parallel states to antiparallel states, which is typical for frame deformations. This process occurs because γ varies from $+\infty$ to 0 and to $-\infty$, and the infinity of γ is provided by the ELs, i.e. the path departs from EL_1 and terminates at EL_2. It is thus understandable that the frame

deformation is a result of hyperbolic transformation, i.e. the Lorentz boost in general relativity [8]. In Region III, the evolution of eigenstates is similar to that in Region I, simply the two eigenstates swap.

In broken phases, the local metrics are both

$$g_{\mathrm{II,IV}} = \begin{bmatrix} 0 & 1 \\ 1 & 0 \end{bmatrix}, \tag{S19}$$

and the evolution of eigenstates is still defined on SO(1,1) group. The difference is that the two eigenstates become complex conjugate, and the frame deformation process is extended to the complex space. Results for path β ($\pi/4 \le \theta \le 3\pi/4$) is provided in Fig. S3c. As shown in Fig. S3c2-c3, the initially parallel eigenstates bifurcate to form a conjugate pair, and finally evolve to two anti-parallel imaginary vectors.

With the above frame deformation process on any of the paths aforementioned, one can already determine that an NIP can be formed by the intersection of the two ELs (or ESs). Hence, an open path joining ELs (or ESs) can provide a lot of information on the intersection of the ELs (or ESs). This is essentially different from isolated singularities, for which a path is only meaningful whenever it is closed. Our former work [10] has established the relation between the frame deformation with the conventional Berry phase, and in the next section we will discuss this accompanied with topologically protected edge states.

4. Topologically protected edge states of NIP

The isolated singularities in band structures (e.g. Dirac/Weyl points or nodal lines) are often accompanied with edge states, which are stable against boundary conditions of the system, and are protected by the non-trivial topology of the singularities. However, the bulk-edge correspondence of hypersurface singularities in non-Hermitian systems has not been discussed. Apparently, it seems impossible to find stable edge states for such singularities, because closed loops circulating them will inevitably traverse ESs and experience real line gap closing. As a matter of fact, hypersurface singularities indeed support topologically protected edge states. In this section, we will provide solid evidence for this counter-intuitive physical phenomenon based on the NIP (or NIL).

We consider the following 1D k-space Hamiltonian corresponding to a lattice model,

$$H(k) = \sigma_z \cos k + i\sigma_y \sin k + v\sigma_0 \cos(k + a) \tag{S20}$$

where σ_0 is the 2 by 2 identity matrix, and the last term proportional to σ_0 is useful in tuning bandgaps so that edge states can be easily found out. As a common fact, introducing the identity term does not change the topology of the system, and the degeneracy features remain unchanged. It is obvious that $f_2(k)=\cos k$ and $f_2(k)=\sin k$, and the Hamiltonian preserves the symmetries in Eq. (1) of the maintext. The trajectory of $(f_2(k), f_3(k))$ encloses the NIP, as shown in Fig. S4a. Such a Hamiltonian can be realized by the 1D periodic system in Fig. S4b, and the corresponding real space Hamiltonian is

$$H_r = \underbrace{\frac{1}{2}(\sigma_z + \sigma_y + ve^{ia}\sigma_0)}_{t_1} \sum\nolimits_j c_j^\dagger c_{j+1} + \underbrace{\frac{1}{2}(\sigma_z - \sigma_y + ve^{-ia}\sigma_0)}_{t_2} \sum\nolimits_j c_j^\dagger c_{j-1} \tag{S21}$$

where j denotes unit cell index, and t_1 and t_2 are both 2 by 2 hopping matrices, with their elements denote hopping parameters between lattice sites (see Fig. S4b). It is shown that the hopping matrices have the following relation.

$$t_1^* = t_2 \tag{S22}$$

Since the loop inevitably traverses the ELs four times, the band structure on the 1D Brillouin zone experience real line gap closing four times, as indicated by Fig. S4c. For the path α residing in Region I, our former result shows that the two initially parallel eigenstates bifurcate and evolve to two anti-parallel states (Fig. S3b2), which is a frame deformation process. This process shows that the relative rotation angle between the two eigenstates is equal to π, which is equal to an integral

$$\psi = \oint_{l_\alpha} i \langle \varphi | \nabla_k \varphi \rangle d\mathbf{k} \tag{S23}$$

The loop l_α in the integration is shown in Fig. S4d, which is simply joining the trajectories of the two eigenvalues on path α at ELs. Therefore, the loop l_α is in the 3D Re(ω)-f_2-f_3 space, not simply confined in the f_2-f_3 plane. It is not difficult to identify that Eq. (S23) is the conventional Berry phase. Thus the frame deformation is related with the conventional Berry phase, relative discussions have already been provided in [10]. On path α', the two eigenstates swaps compared with path α, and thus the relative rotation angle is –π, meaning that the Berry phase along the loop $l_{\alpha'}$ is –π (see Fig. S4d). In addition, the identity term in the Hamiltonian (Eq. S20) introduces a real line gap between the eigenenergies on path α and path α'. Resultantly, if we truncate the 1D system with open boundaries, there will be a pair of edge modes (the truncated system has two edges) residing in the line gap, as shown in Fig. S4e. Here OBC stands for open boundary condition, and PBC stands for periodic boundary condition. Since the eigenenergies in broken phases have point gaps, skin effect also arises, as indicated in Fig. S4e. The edge states are away from any bulk modes and skin modes, and thus skin modes and edge modes can be easily distinguished. The field distribution (amplitude $|\varphi|$) of one edge mode is shown in Fig. S4f, where *Ns* denotes lattice sites. To obtain the eigenenergies and eigenstates under OBC, we simply write down the truncated real space Hamiltonian with finite unit cells (here we preserve 300 unit cells), and numerically solve the eigenvalue problem of the real space Hamiltonian.

5. Some other nontrivial loops in parameter space

In Fig. 2 of the maintext, we introduced some typical nontrivial loops and the corresponding topological invariants. Since the number of elements in the group (Eq. 4) is infinitely large, and some elements other than Fig. 2 is also useful, here we give a brief introduction on these invariants and the corresponding path combinations in parameter space.

Figure S5(a) shows the path product $\alpha'\beta$. Note that the basepoint has been fixed at A (or A'), and thus we cannot exchange the order in the product (i.e. $\beta\alpha'$). Exchanging the order in the product means that the basepoint is changed from A (or A') to B (or B'). In homotopy theory, one will obtain another fundamental group by changing the basepoint without changing the order parameter space, and the groups obtained by changing the basepoint are isomorphic to each other since the quotient space M is path-connected. It is not difficult to find out that $\alpha'\beta=\alpha'\alpha^{-1}\alpha\beta$, and thus the corresponding topological invariant is $Z_2^{-1}Z_1$, which is an element of the group (Eq. 4). The path combination $\beta'^{-1}\beta$ is totally in broken phases, and is a counterpart of Fig. 2(b). Since $\beta'^{-1}\beta$ can be obtained as the path product $\beta'^{-1}\alpha'^{-1}\alpha'\alpha^{-1}\alpha\beta$, it is thus obtained that the invariant on the loop is $Z_3^{-1}Z_2Z_1$. In a similar way, the path combination in Fig. S5(c) $\alpha\beta'$ can be obtained as the product $\alpha\alpha'^{-1}\alpha'\beta'$, and the invariant on the loop is simply $Z_2^{-1}Z_3$.

6. k-space Hamiltonian matrix of the lattice model

In the maintext, we provide a lattice model to show that such Hamiltonians can be realized by non-reciprocal hoppings. We also illustrated that the chain of CILs can be formed because it is protected by the squared invariants $(Z_1Z_3)^2$ [or $(Z_1^{-1}Z_3^{-1})^2$] and the trivial invariant (on the blue loop) (see Fig. 4c in the maintext). The intersection chain (denoted by the black arrows in Fig. 4c) points are also protected by the mirror symmetries $k_x+\pi/d\rightarrow -k_x+\pi/d$ and $k_y\rightarrow -k_y$ for E_0=0. Breaking the mirror symmetries (setting E_0 to be nonzero) will open the chain points but will not affect the topology on the blue and orange loops. Here we provide the **k**-space Hamiltonian of the lattice model. Firstly, the real space Hamiltonian can be transformed to a **k**-space Hamiltonian by performing Fourier transformation (setting the length of bond vectors d=1),

$$\begin{aligned} H_1 = & t_1(e^{ik_x}+e^{-ik_x}+e^{ik_y}+e^{-ik_y}+e^{ik_z}+e^{-ik_z})a_{M,k}^{\dagger}a_{N,k}-h.c. \\ & +E_0(a_{M,k}^{\dagger}a_{M,k}-a_{N,k}^{\dagger}a_{N,k}) \\ & +t_2(e^{ik_x+ik_y}+e^{-ik_x-ik_y}-e^{ik_x-ik_y}-e^{-ik_x+ik_y})(a_{M,k}^{\dagger}a_{M,k}-a_{N,k}^{\dagger}a_{N,k}) \end{aligned} \tag{S24}$$

By diagonalizing Eq. (S24), we obtain

$$H_1(\mathbf{k})=\begin{bmatrix} E_0+2\sin k_x \sin k_y & \cos k_x+\cos k_y+\cos k_z \\ -\cos k_x-\cos k_y-\cos k_z & -E_0-2\sin k_x \sin k_y \end{bmatrix} \tag{S25}$$

Hence, it can be expanded with Pauli matrices $i\sigma_2$ and σ_3 [with $f_3(\mathbf{k})=E_0+2\sin k_x \sin k_y$ and $f_2(\mathbf{k})=\cos k_x+\cos k_y+\cos k_z$, see Eq. (2) in the maintext], preserving the symmetries in Eq. (1).

References:

[1] A. Mostafazadeh, Pseudo-Hermitian representation of quantum mechanics, Int. J. Geo. Meth. Mod. Phys. **7**, 1191-1306 (2010).

[2] R. Zhang, H. Qin, J. Xiao, PT-symmetry entails pseudo-Hermiticity regardless of diagonalizability, J. Math. Phys. **61**, 012101 (2020).

[3] A. Mostafazadeh, Pseudo-Hermiticity versus PT-symmetry III: Equivalence of pseudo-Hermiticity and the presence of antilinear symmetries, J. Math. Phys. **43**, 3944-3951 (2002).

[4] Ş. K. Özdemir, S. Rotter, F. Nori, et al. Parity–time symmetry and exceptional points in photonics[J]. Nat. Materials **18**, 783-798 (2019).

[5] E. H. Spanier, Algebraic topology, Springer Science & Business Media, 1989.

[6] P. Gajer, The intersection Dold-Thom theorem, Topology **35**, 939-967 (1996).

[7] W. Ebeling, The monodromy groups of isolated singularities of complete intersections, Springer, 2006.

[8] D. Z. Freedman, A. Van Proeyen, Supergravity, Cambridge university press, 2012.

[9] T. Frankel, The geometry of physics: an introduction, Cambridge university press, 2011.

[10] J. Hu, R. Y. Zhang et al. Non-Hermitian swallowtail catastrophe revealing transitions across diverse topological singularities, Research Square preprint [https://doi.org/10.21203/rs.3.rs-1853770/v1] (2022).

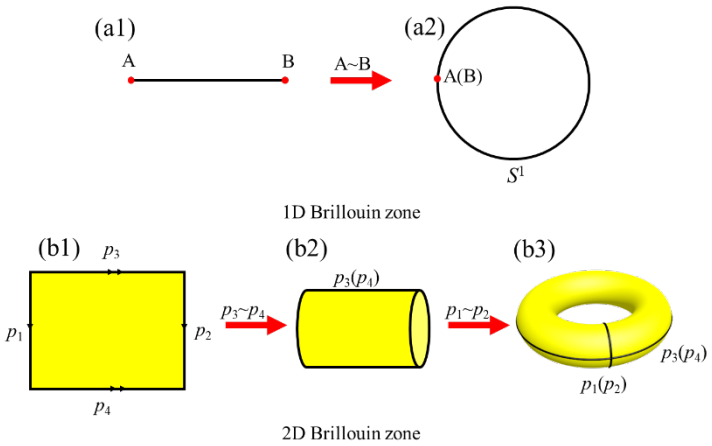

Fig. S1. Quotient space of momentum space in periodic systems. (a1)-(a2) The quotient space of 1D Brillouin zone is a circle (S^1) by identifying the two points on the Brillouin zone boundary. (b1)-(b3) Construction of quotient space of 2D Brillouin zone. Identifying the boundaries p_3 with p_4 gives a cylinder, which becomes a torus by identifying p_1 with p_2.

$$V := \mathbb{R}^2$$

$$S := \{\mathbb{R}^2, > \{|\, f_2 \,| = |\, f_3 \,|\}, > \{f_2 = f_3 = 0\}\}$$

$T_1 :=$ $\mathbb{R}^2$

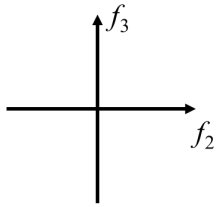

$T_2 :=$

$T_3 :=$

Fig. S2. Stratified space of the 2D plane with ELs and NIP.

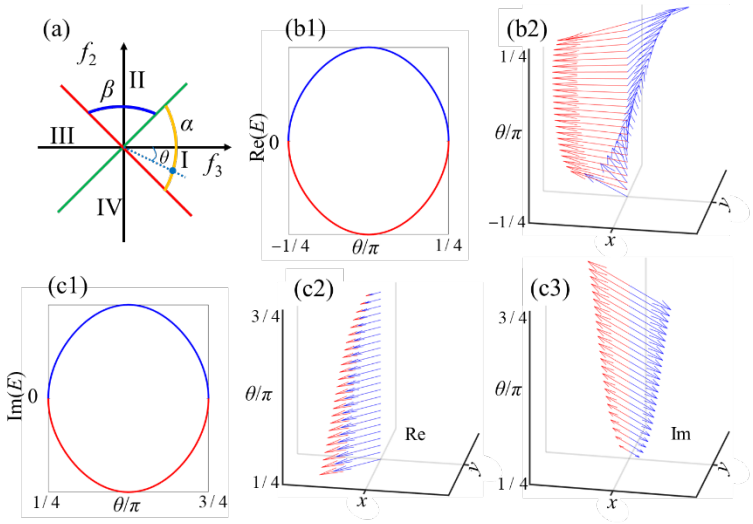

Fig. S3. Frame deformation along different paths. (a) Paths α and β in parameter space. θ denotes the path parameter, i.e. f_3=cosθ, f_2=sinθ, $-\pi/4 \le \theta \le \pi/4$ for α, $\pi/4 \le \theta \le 3\pi/4$ for β. (b1-b2) Evolution of eigenvalues (real part, b1) and eigenstates along path α. (c1-c3) Evolution of eigenvalues (imaginary part, c1) and eigenstates (c2, real part; c3, imaginary part) along path β.

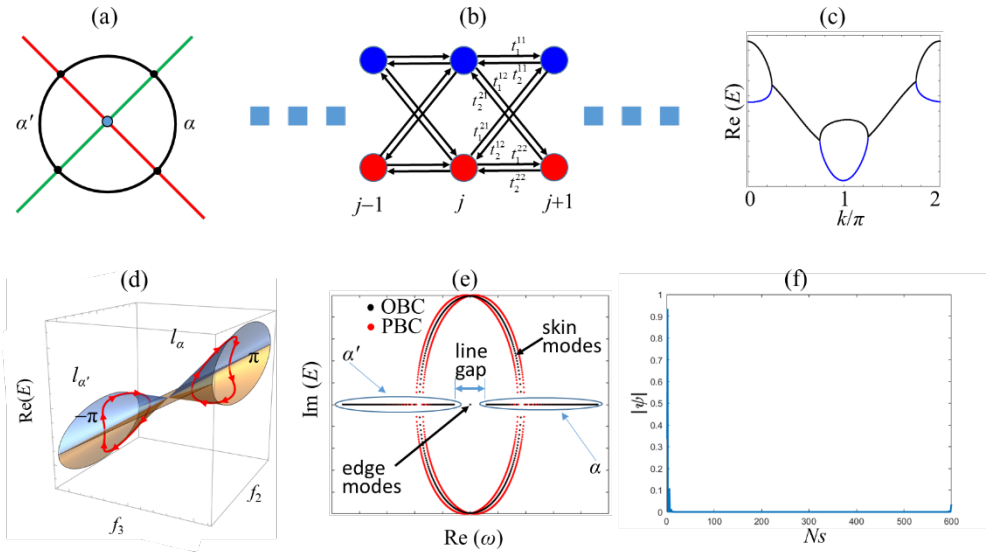

Fig. S4. Topologically protected edge states of NIP. (a) A loop circulating the NIP, being the Brillouin zone of the 1D lattice model in Eq. S12, is partitioned into four paths, with α and α' residing in exact phases. (b) Realization of the lattice model. (c) Eigenvalue dispersions (real part) of the model Eq. S20. (d) Joining the trajectories of two bands on path α forms a loop in Re(ω)-f_2-f_3 space l_α, along which the Berry phase is π. For path α', joining the two bands forms the loop $l_{\alpha'}$, along which the Berry phase is –π. (e) Eigenvalues of the model with open boundary conditions (OBC) and periodic boundary conditions (PBC). There exist a pair of edge modes in the line gap for eigenstates on paths α and α'. (f) Field distribution of one edge mode. The lattice model with OBC has 300 periods (600 lattice sites).

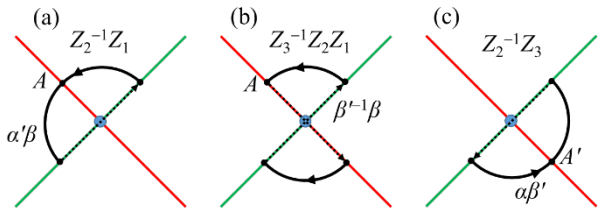

Fig. S5. Some other nontrivial loops and the corresponding topological invariants (other than Fig. 2) taking from the group Eq. 4.